Chapter 5

Arbitrary Form Plasmonic Structures: Optical Realization, Numerical Analysis and Demonstration Applications

Quang Cong Tong, Fei Mao, Mai Hoang Luong, Minh Thanh Do, Rasta Ghasemi, Tran Quoc Tien, Tho Duc Nguyen and Ngoc Diep Lai

Additional information is available at the end of the chapter

http://dx.doi.org/10.5772/intechopen.79236

Abstract

Surface plasmon resonance has attracted more and more attention thanks to its wide range of applications in numerous fields (physics, chemistry, biology, etc.). In this chapter, we present different aspects, from theoretical calculation and experimental fabrication to applications demonstration, related to arbitrary shape plasmonic nanostructures. First, numerical calculations based on finite-difference time-domain method were realized to investigate the plasmonic properties of gold nanostructures having various size and shapes. Then the direct laser writing method was demonstrated as an excellent tool for fabrication on demand of arbitrary nanostructures. Plasmonic structures were obtained indirectly by a standard lift-off method from a polymeric template and directly by tightly focusing a continuous-wave laser beam onto a metallic thin film. Finally, demonstration of various applications of fabricated plasmonic structures, namely plasmonic-based data storage, color nanoprinter, tunable filters, and plasmonic-magneto-optics sensors will be shown.

Keywords: plasmonics, direct laser writing, one-photon absorption, tunable filter, data storage, color printer, sensor

1. Introduction

Since the first scientific observation by Wood in 1902 [1], surface plasmon resonance (SPR) has attracted considerable interest in different domains: physics, chemistry, biology, and so

on [2–4]. The physical phenomenon of SPR is arisen by light-matter interaction at the interface of metallic and dielectric materials, especially in noble metals, for example, silver and gold [2–4]. The physical mechanism of the SPR can be briefly explained as following. Under irradiation of an electromagnetic (EM) wave, the free electrons in metallic materials are driven to oscillate at the frequency of the external EM field. This electron oscillation at the metallic surface causes a charge separation with respect to the ionic lattice, forming a dipole oscillation along the direction of the electric field of the light. The amplitude of the oscillation reaches maximum at a specific frequency, called SPR frequency, when the incident EM frequency matches the eigenfrequency that relates to the restoring force stemming from the lattice of positive nuclei. For a metallic object with finite dimension, only the electrons on its surface are the most significant since the EM wave can only penetrate a limited depth in metal. Therefore, the collective oscillations of such electrons are called SPR [2].

The SPR band intensity and spectra depend on several factors affecting the electron charge density on the metallic surface, such as the metal type, the dielectric constant of the surrounding medium, particle size, shape, structure, and composition [5]. The plasmonic structures are therefore distinguished into three categories: (i) surface plasmon polariton; (ii) localized surface plasmon resonance; and (iii) plasmonic nano-structures.

Surface plasmon polaritons (SPPs) are EM excitations propagating along the interface between a dielectric and a metal. These EM surface waves arise via the coupling of the EM field to oscillations of the conductor's electron plasma. As a SPP loses energy to the metal due to absorption and scattering, it can only propagate for a finite distance along the interface. Likewise, perpendicularly to the interface, electric field falls off evanescently and can only penetrate into the metal a certain tiny "skin depth" [2], while such an evanescent electric field extends more in the dielectric. Therefore, SPPs are very sensitive to any perturbation within the skin depth and are often used as a very sensitive chemical, biological, or gas sensor [6].

In contrast to SPP, localized surface plasmon resonance (LSPR) occurs when collective oscillations of free electrons are confined to a finite volume, such as metal nanoparticles (NPs), as EM standing waves. The LSPR is excited when the frequency of the incident photons matches the resonance frequency of the NPs. Generally, the LSPR in visible range is obtained with noble NPs with dimensions below 100 nm. The plasmonic properties of metallic NPs vary with their shape and size and are also affected by the refractive index of the surrounding medium. This results in various applications of metallic NPs in different domains, from fundamental science to practical applications [7].

Clearly, the LSPR can strongly and locally amplify the EM field near the metallic surface. It is recently demonstrated that this effect becomes much stronger when two or multiple metallic nano-objects are arranged very close to form the so-called plasmonic nanostructure (PNS) [8]. Two NPs, for example, under an EM illumination can be described as two point dipoles. When (i) NPs are closely spaced (separation $\ll$ light wavelength) and (ii) light polarization is appropriated (longitudinally), these two point dipoles can interact via their near-fields: the restoring force acting on the oscillation electrons of each NP is increased by the charge distribution of their neighboring NP. Therefore, EM field in between this "dimer" can be locally and intensely enhanced, resulting in a hotspot [9]. Following this idea, the plasmonic

effect can be also amplified and coupled in an aligned array of metallic NPs (NPA) [10]. A prominent example for coupled SPP nanostructures (NSs) is a nano-hole array (NHA), which is considered as an inverse structure of an NPA [11]. In such a system, the SPP can propagate throughout the NHA surface thanks to the coupling of multiple nano-holes perforated appropriately in a metallic thin film. The properties of plasmon resonance of NHAs and NPAs can be tuned by characteristic length scales and types of arrays such as periodic, quasiperiodic, and aperiodic structures. Such PNSs have great promise for many interesting applications, such as tunable filter and nano-scaled color printing [12].

This chapter deals with different aspects, from theoretical calculation and experimental fabrication to applications demonstration, of two last kinds of SPR, namely, LSPR of metallic NPs and SPP coupling of metallic NHAs. In the first section, numerical calculations based on finite-difference time-domain method will be used to investigate the plasmonic properties of different metallic NSs. We first demonstrate LSPR in individual NPs and show strong relations of plasmon-optical properties on the sizes and shapes of NPs and surrounding media. We also demonstrate a quasi-complete work of gold NHAs for optical bandpass filter and sensing applications. Then, the use of direct laser writing (DLW) technique will be presented in detail, as an excellent method for realization of PNSs on demand. Two practical ways will be demonstrated indirectly via the use of a polymeric template and directly by using an optically induced thermal effect. The advantages of this DLW fabrication method will also be discussed and compared with other fabrication techniques. Finally, plasmonic applications of fabricated PNSs, namely plasmonics-based data storage, color nanoprinter, tunable filters, and plasmonic-magneto-optics sensors will be demonstrated and discussed.

In the last section, some conclusions of the newly developed plasmonic structures and fabrication technique, advantages this technology brings to the plasmonic/nanophotonic field, as well as some prospects, will be shown.

2. Numerical investigation of plasmonic nanostructures

Since the discovery of the plasmonic effect, many text books have been produced [2, 13–16] and the theory of this interesting effect can be found easily. We present here only a numerical method to model the analytical theories, especially for some particular plasmonic structures. Actually, there exist different simulation methods which allow to create models of an arbitrary plasmonic structure and to obtain its plasmo-optical properties. Each method presents its own advantages and disadvantages, such as required time processing, computer memory, and simulation precision. We have adopted a very well-known simulation method, which allowed us to achieve rapidly and precisely the plasmo-optical properties of any metallic NSs.

2.1. Simulation methodology

Finite-difference time-domain (FDTD) is a numerical analysis method allowing to obtain approximate solutions of electrodynamics problems. FDTD workground was first set in 1928 [17]. However, it only became popular since the1980s thanks to the revolution of information

technology [18]. Recently, with the assistance of modern computers, FDTD has become a powerful technique for researchers to predict the EM response of any structure, in particular PNSs. As other finite-difference modeling methods, FDTD is grid-based. It means that computational domains will be meshed into minor units, mostly in a cube shape, with associated vector components of the electric (**E**) field and magnetic (**H**) field, which are determined by Maxwell's equations. In simulation, the **E** and **H** fields are calculated at every point in space, forward in time. Additionally, FDTD is a time-domain method, so it can cover a wide range of frequencies with a single simulation run [19]. Thanks to these advantages, FDTD provides us a natural way to treat any electrodynamics problem, especially periodic structures and broadband sources in PNSs complications.

For calculation of plasmonic properties of all gold (Au) nanostructures (NSs) presented in this chapter, we have performed simulations by using the FDTD method (Lumerical software). **Figure 1** shows the FDTD simulation model. The simulation area was bounded in x- and y-directions by parallel planes in which periodical boundary conditions are defined, while perfectly matched layer metal boundary conditions were applied in top and bottom boundaries to prevent any reflections. The absorbance spectra were calculated from Fourier transform time-dependent transmission monitor. These metallic NSs could be computationally created or imported from real structures, which are reconstructed by using the scanning electron microscope (SEM) and atomic force microscope (AFM) data. Indeed, by using Lumerical software, it is possible to construct models for single or multiple NPs, with changeable particle parameters (size, shape, materials, compositions, etc.). It is also able to simulate NPs organized in order, such as dimer and arrays, with uniform distribution or random distribution. This software also allows to import real SEM and AFM images to simulate with true fabricated structures. Other FDTD model parameters are set as close to characterization conditions: the optical properties of materials were taken from [20] for SiO_2 substrate and from [21] for Au thin films.

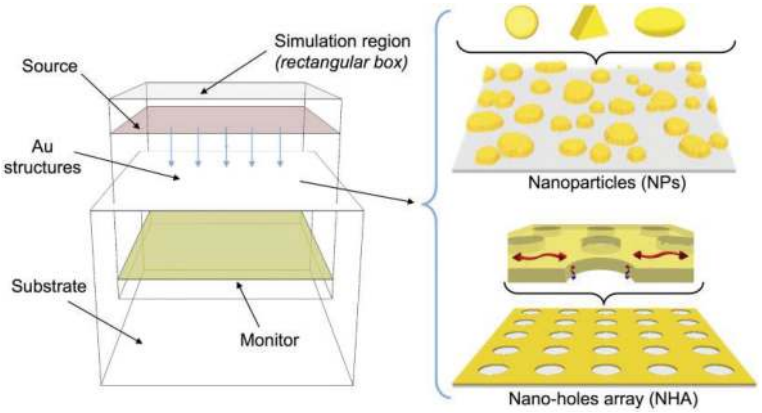

Figure 1. FDTD model used to simulate the plasmonic properties of Au NSs, including Au NPs of different shapes and Au NHAs. These NSs could be computationally created or imported from real structures, which are reconstructed by using SEM and AFM data.

http://dx.doi.org/10.5772/intechopen.79236

2.2. Localized surface plasmon resonance

Au NPs possessing particular shapes, such as nano-sphere, nano-rod, and nano-prism, are often fabricated by standard chemical methods, for example, the Turkevich [22], Brust [23] seeded growth [24] or other miscellaneous methods [25]. Those NPs are usually randomly distributed and initially suspended in a solvent such as water. Therefore, they are totally independent, that is, the plasmonic resonance is purely localized and uncoupled. To study the plasmon effect of Au NPs, a simple model consisting of a single NP is demonstrated. The simulation region is a $1 \times 1 \times 1\ \mu m^3$ box with perfectly matched layer boundary conditions (PML BCs) for all x-, y-, and z-axis. The mesh size of $1 \times 1 \times 1\ nm^3$ is set in the region encompassing the Au NP and Au-medium interface.

The plasmon resonance frequency is highly sensitive to the refractive index (n) of the surrounding environment. Hence, a change of n results in a shift in the resonant frequency. We have considered a spherical Au NP immersed in various media, such as air, water, or glass. As n near the NP surface increases, the absorption coefficients increase and the absorption spectrum shifts to longer wavelengths as shown in **Figure 2(a)**. Theoretically, this means that the LSPR peak location will be red-shifted if the surrounding medium changes from air to water and to oil.

Optical properties of Au NPs can also be tuned by varying their sizes and shapes. **Figure 2(b)** shows the calculated absorption spectra of Au nano-rods with different aspect ratios (the diameter a was fixed at 15 nm, and the ratio R = 1, 2, 2.5, and 3). We can see that the longitudinal mode, which is commonly referred to the plasmonic band induced by exciting along the long axis of nano-rods, is significantly red-shifted, while the transverse mode, which is commonly referred to the plasmonic band when exciting along the short axis, exhibits a slight blue shift as the aspect ratio R increases.

Consider now another kind of NP, namely Au nano-prism. The size and shape dependence of plasmonic band can also be seen clearly in this case. The LSPR position is highly sensitive to the edge length and the aspect ratio (defined as the ratio d/t between the edge length, d, and

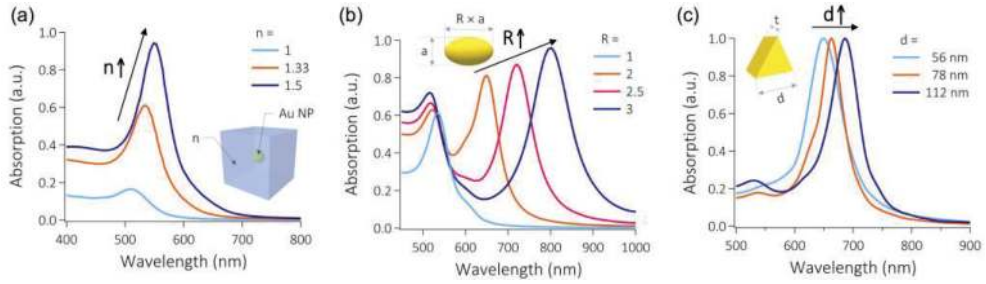

Figure 2. (a) Numerical calculation of absorption spectra of Au NPs (diameter d = 50 nm) in different media (air, water, and glass, indicated by its refractive index, n = 1, 1.33, and 1.5, respectively). Inset: Illustration of a single Au NP in a medium with refractive index n. (b) Calculated absorption spectra of Au nano-rods in water with different aspect ratios, R. The diameter of the Au nano-rod is fixed at a = 15 nm. Inset: design of Au nano-rod. (c) Size-dependent absorption spectra of Au prism in water, calculated with different edge-lengths, d. The thickness of the Au prism is fixed at t = 25 nm. Inset: design of Au nano-prism.

thickness, t, of nano-prisms). The larger edge lengths and higher aspect ratio generally result in red shifted resonances. The red shift of the position of the peak maxima (from 642 to 684 nm) corresponds to the edge length of Au nano-prism increases (from 56 to 112 nm) as illustrated in **Figure 2(c)**. This result is quite interesting as compared to that obtained by a spherical NP having a similar size. That allows to easily create different colors by using metallic NPs with different shapes.

From three examples of nano-sphere, nano-rod, and nano-prism, there exists thus a strong dependence of the LSPR peaks (number of modes, location, and intensity) on metallic NPs shape, size, and surrounding medium. Generally, a red shift of absorption spectrum is noticed when NPs size increases. In addition, increment of surrounding refractive index can increase absorption coefficient and enlarge red-shift absorption spectrum. This general observation gives us an insight to construct a numerical model for multiple-sizes/shape nano-islands (NIs) as well as to qualitatively explain their use as plasmonic sensors and/or data storage and color nanoprinter.

2.3. Surface plasmon resonance of randomly distributed Au nanoparticles

Another method, called thermal annealing dewetting technique [19, 26, 27], has recently been demonstrated as an excellent way to produce monolayers of randomly distributed Au NPs on a substrate. In this technique, discontinuous thin metallic films are first deposited on a substrate, such as a glass, and then annealed at a temperature of about 500°C. The discontinuous metallic films are thermally melted resulting in isolated metallic NIs. In this case, it is not correct if one calculates the plasmonic properties of only a single NP but it should be done for an ensemble of NPs of various sizes. There exist a few of works in literature, which attempted to model the optical properties of a monolayer of Au NIs [28, 29]. However, most of the works were based on statistical methods to estimate the median parameters of NIs, which required a lot of raw data and statistical analysis efforts. Moreover, in order to simplify the models, an assumption of semispherical NIs was generally used, which might greatly alter the final calculation results since LSPR is highly sensitive to size and shape of NIs.

The calculation method shown in **Figure 1** allowed thus solving completely the problem. This process required only a SEM image and an AFM image. SEM image is utilized to extract the top-view sizes/shapes and (x,y) position coordinates of NIs. This two-dimensional (2D) map is then extruded to three-dimensional (3D) structures with the estimated height from AFM data. **Figure 3** shows the plasmonic resonant spectra of monolayer films of Au NIs with different average NIs sizes. The plasmonic peak located around 550 nm is clearly evidenced. When the particles size increases, the corresponding resonant peaks of the absorption spectra are red-shifted. Theoretically, the resonance peak shifts by a quantity of about 48.5 nm when the average size of NIs changes from 20 to 100 nm. This shift suggests that the structuration of Au NPs by the dewetting method can be a good idea for applications such as tunable absorbers and color nanoprinter.

2.4. Surface plasmon resonance in periodic Au nano-holes array

Recently, several strategies have been employed to realize a metallic optical filter, including plasmonic resonators [30], plasmonic metasurfaces for perfect light absorption [31],

http://dx.doi.org/10.5772/intechopen.79236

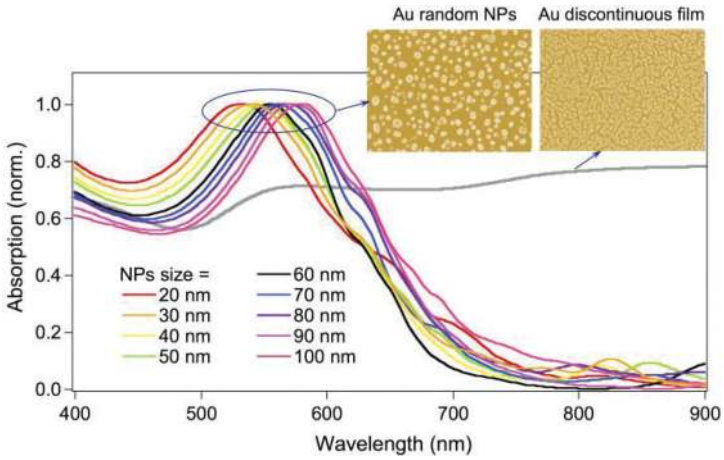

Figure 3. Simulation result of absorbance spectra of Au NPs randomly distributed on glass substrates. Different curves correspond to samples having different average NPs sizes. Insets show SEM images of a thin film Au sample obtained before annealing, corresponding to the absorption spectrum of gray color, and of an Au NPs sample obtained after thermal annealing, corresponding to one of the plasmonic resonance absorption spectra.

plasmonic-photonic crystal cavity [32], grating coupler with waveguide resonant grating [33], and so on. In this section, Au NHAs are demonstrated theoretically as an excellent optical bandpass filter via the well-known extraordinary optical transmission (EOT) phenomenon [34]. For complete simulations of NHAs, the parameters were selected and categorized into two groups as described below:

Fixed parameters: NHA structures with round holes were chosen because it is the most similar to the structure fabricated by direct laser writing lithography, which will be shown in the fabrication section. The optical constants of silica, Au, and Cr were taken from [20, 21], respectively. Note that Cr is usually used for enhancing the adhesion of Au material with substrates, and it should be thin to avoid the influence of plasmonic properties of Au structures. The periodicity of NHAs was fixed at 1000 nm. The net transmission light was calculated using the arithmetic average of the simulation results of individual and orthogonal polarizations.

Swept parameters: the thickness of Au layer and Cr layer were swept from t_{Au} = 10 to 90 nm and t_{Cr} = 0 to 20 nm, respectively. Diameter of the hole was also varied from d_{hole} = 300 to 900 nm. In addition, monitors were set within computation domain to analyze transmission spectra along with EM field distributions. Results were normalized to the transmission spectra obtained from a glass substrate (no NHA) and evaluated right after each simulation to confine the parameters, with a purpose of the fastest convergence.

Figure 4 shows calculated transmission spectra of Au NHA as a function t_{Au}, t_{Cr}, and d_{hole}. As can be seen in **Figure 4(a)**, the EOT peak position and width depend strongly on the thickness of Au NHA. In detail, this peak was blue-shifted and became shaper when the Au thickness increased. In contrast, an increase of Cr layer thickness suppresses the transmission peaks dramatically (**Figure 4(c)**). Another parameter, which influences greatly the transmission spectrum, is hole diameter, d_{hole}. Bigger holes allow higher transmission coefficients; however,

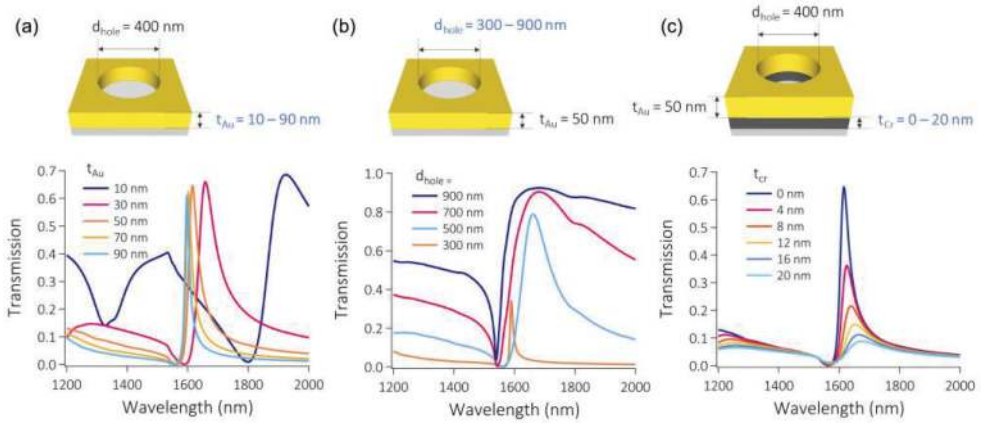

Figure 4. Calculated transmission spectra of Au NHAs as a function of Au layer thickness, t_{Au} (a); of nano-hole diameter, d_{hole} (b); and of Cr layer thickness, $t_{Cr,}$ (c), respectively.

band selection is poor. Conversely, smaller holes allow fewer transmission resonance modes, which make transmission peak sharper but also decrease the transmission coefficients. Based on this insight along with advantages and disadvantages of the direct laser writing method, an optimum NHA should have the following parameters: t_{Au} = 50 nm, t_{Cr} = 3 nm, Λ = 1000 nm, and d_{hole} = 400 nm, respectively.

3. Realization of desired plasmonic nanostructures

Different fabrication methods of PNSs have been demonstrated, each possessing its own advantages and drawbacks. For each application, particular metallic NPs or PNSs are required and then a specific fabrication method could be adopted. To form Au NPs and NSs in a small area but with a desired configuration, electron-beam lithography [35, 36] and direct laser writing (DLW) method [37] are two best choices and both are commercially available. Generally, these two methods allow creating PNSs by an indirect way, namely, PNSs are obtained by evaporation of metals on polymeric templates and lift-off. Recently, a direct fabrication method was also demonstrated by using optically induced thermal effect via DLW technique [38]. In this section, the use of DLW will be presented in detail for realization of desired PNSs indirectly and directly.

3.1. Direct laser writing method

Figure 5(a) illustrates the experimental setup of the DLW system. For realization of 2D PNSs, this DLW involves with a one-photon absorption (OPA) mechanism by using a continuous-wave (cw) laser beam. The sample is a commercial positive photoresist, S1805, for fabrication of PNS by the indirect way. This setup is also used to realize PNSs by the direct way using a sputtered Au film sample. The laser beam, whose wavelength (532 nm) locates the absorption

http://dx.doi.org/10.5772/intechopen.79236

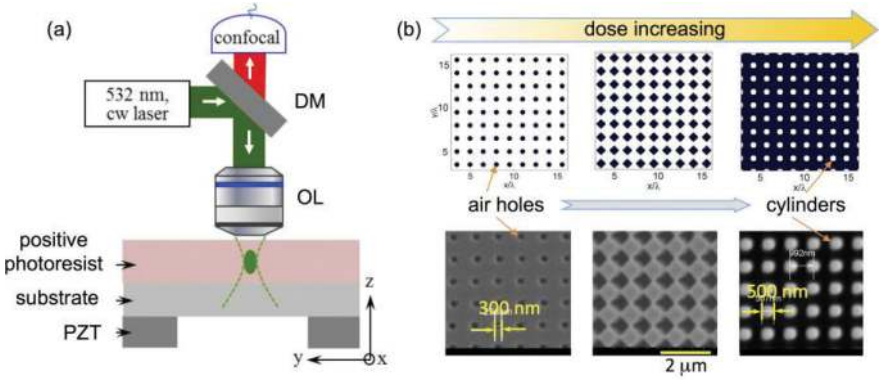

Figure 5. (a) Illustration of the DLW technique used to realize arbitrary 2D structures on photoresist and Au film. PZT: piezoelectric translator; DM: dichroic mirror; OL: objective lens. (b) Control of filling factor of structures fabricated on a positive photoresist by adjusting the exposure dose. A 2D square structure is obtained by scanning continuously the focal spot in x- and y-directions. Top: theoretical light pattern; bottom: experimental demonstration. The separation between lines, that is, the period of structure, is $\Lambda = 0.8$ μm, and the structures change from negative (air-holes) to positive (polymeric cylinders) forms.

spectrum of both S1805 and Au materials, is tightly focused into samples by a high numerical aperture (NA) objective lens (OL). Since the DLW operates with an OPA mechanism, the required laser power is very modest, in the range of few microwatts for S1805 photoresist and a few dozens of milliwatts for Au films. Thanks to the use of a high NA OL, the light intensity at the focusing region is, however, very high, which is enough for depolymerizing the S1805 photoresist and thermally dewetting the Au films. 3D piezoelectric translator (PZT) connected to a computer control allows the focusing spot to move through the sample following a desired trajectory. By controlling the laser power and the exposure time, the exposure doses are adjusted resulting in structures with desired sizes and forms, as illustrated in **Figure 5(b)**. A detection system consisting of a lenses ensemble, a pinhole, and an avalanche photodiode is used to determine the focusing position, which should be practically located on substrate surface. It should be noted that this DLW is time consuming, like e-beam lithography. Also, in order to keep high resolution, the total area of fabricated structures is limited, generally of about 100x100 μm^2. This surface should be enough for various applications, and in case necessary, it could be enlarged by using a PZT with a larger scanning range, together with an increase of fabrication time.

3.2. Realization of plasmonic structure by an indirect method

The indirect fabrication of PNSs consists of two steps: (i) fabrication of photoresist templates by DLW method and (ii) transferring templates to metallic structures by evaporation of method and template lift-off. **Figure 6(a)** illustrates the fabrication process of Au NSs by this indirect method. This process is very similar to the fabrication of PNSs by e-beam lithography [35–37]. To fabricate desired structures, the positive photoresist was first coated on cleaned glass substrates and exposed by the DLW system. The samples were then developed, removing all exposed parts and leaving unexposed parts as desired structures. It is demonstrated

that the final structures depend strongly on the exposure dose, that is, the laser intensity and the exposure time. Therefore, the filling factor is controlled precisely and both air-holes and dielectric-cylinder structures can be easily and reliably realized (**Figure 5(b)**).

The thin Au film (typical thickness is about 50 nm) is then deposited on the top surface of the polymeric structures by a thermal evaporation technique. As indicated previously, a thin layer of Cr (3 nm) was sputtered in between polymeric templates and the Au film in order to enhance the adhesion of the Au film. The samples were then immersed in acetone to remove the polymeric template, leaving the Au PNSs.

Figure 6(b)–(d) shows some examples of 2D PNSs. Depending on the polymeric templates, it is possible to obtain both Au films containing air-holes, that is, NHAs and Au microdisks. The minimum size of the Au microdisks or air-holes is about 300 nm, which is larger than the size limit (about 100 nm) of the polymeric structure fabricated by the DLW. That is because when the polymeric holes or cylinders are small (100 nm), their walls are not vertical and the evaporated Au film is connected between the top and bottom parts of the polymeric structures, influencing the lift-off process. Besides, due to the diffraction limit of the DLW system and also the quality of the positive photoresist during development process, the size of fabricated metallic structures is still large, as compared to those realized by the e-beam lithography technique. A strong effort is currently being made to realize polymeric structures with smaller size and vertical wall, by using, for example, an OL having higher NA, a super-resolution technique to reduce the focusing spot, or a laser with shorter wavelength. Finally, as the most major advantage of the DLW, arbitrary Au NSs can be also realized as shown in **Figure 6(d)**.

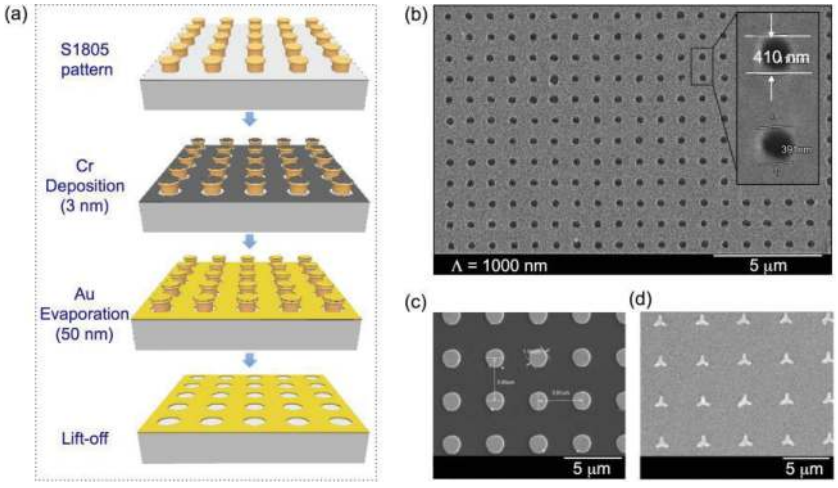

Figure 6. (a) Fabrication of plasmonic structures by using polymeric templates. The S1805 structures with controllable period and filling factor are fabricated by the DLW technique. Plasmonic structures are then obtained by a combination of Au evaporation and lift-off techniques. (b–d) SEM images of experimental plasmonic structures: (b) 2D periodic air-holes Au array; (c) periodic array of Au submicrometer disks; (d) arbitrary Au structure.

3.3. Direct laser writing of gold nanostructures

In Section 2.3, it is shown that the thermal annealing dewetting technique is a simple and cheap way to realize Au NSs [19, 26, 27]. Conventionally, the dewetting effect is performed on a hot plate or in an oven with an annealing temperature of about 500°C, which results in a large Au NIs areas. In the above section, it is demonstrated that that DLW is a very efficient method that allows the realization of any NS on demand. Recently, this technique is also demonstrated as an excellent method to realize PNSs consisting of Au NPs [38]. For that, the DLW technique employed a cw laser to generate a strong and local heating effect in Au material. This is called optically induced thermal effect by the DLW. This opens up numerous applications of PNSs, which could be experimentally achievable at low cost.

A theoretical model is proposed to investigate the optically induced thermal effect at the focusing spot of the optical system. Physically, due to the strong absorption of the Au material at the excitation wavelength and thanks to the optical intensity distribution, a temperature distribution is produced at the focusing region. **Figure 7** illustrates a tightly focused light beam inside an absorbing medium and the light intensity distribution as well as the heat profile at the focusing region. The light intensity distribution (**Figure 7(b)**) is rigorously calculated by using the vector Debye method [39]. By using finite element method with MATLAB PDE solver, the thermal effect model is numerically solved providing the heat profile as shown in **Figure 7(c)**. By using a DLW method with a cw laser, it is theoretically demonstrated that the induced temperature at the focusing spot rises up quickly as a function of exposure time

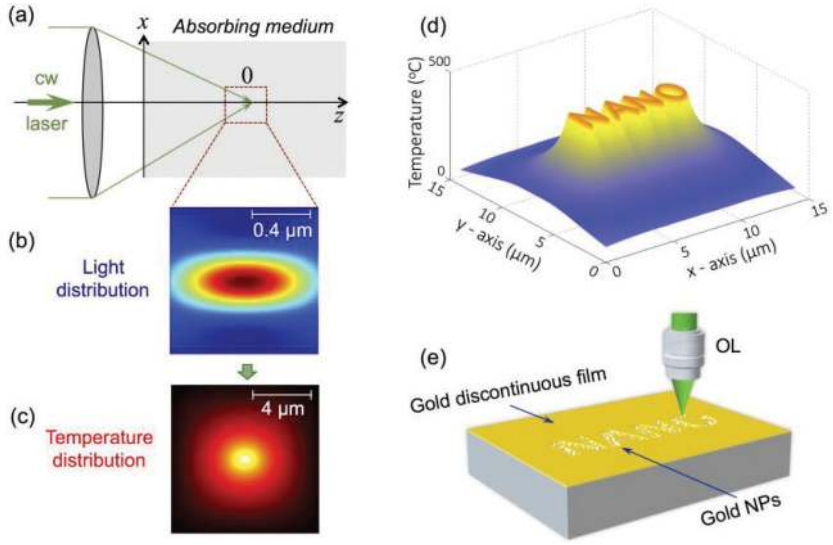

Figure 7. (a) Illustration of a tightly focused light beam inside an absorbing medium. (b) Theoretical calculation of light intensity distribution in xz-plane at the focal region of a high NA OL. (c) Corresponding temperature distribution at the focal region. (d) Temperature pattern (NANO letter) obtained by scanning the focusing spot in xy-plane. (e) Illustration of the formation of arbitrary Au NSs by optically induced thermal effect.

and reaches a stable temperature, approximately 500°C, with an excitation laser power of 40 mW. By moving the focusing spot following a desired trajectory, it is possible to create an arbitrary pattern, such as the "NANO" letter as shown in **Figure 7(d)**. This high temperature can significantly change the morphologies and optical responses of the Au thin film [38]. This thus allows one to realize in a direct way the desired PNSs.

The DLW setup used to directly realize PNSs is same as that illustrated in **Figure 5(a)**, except that the photoresist sample is replaced by a sputtered Au thin sample. These samples were prepared on pretreated glass substrates by a magnetron sputtering technique, with an Au thickness of about 12 nm. The laser focusing spot is moved in 2D space (xy-plane) following a desired trajectory. The typical laser power is a range of 40 mW, which results in a local light intensity of about 10^{11} W/m^2. This high intensity induces a local temperature of about 500°C, which could then locally form Au NIs via the dewetting effect. Using an appropriate laser power, the reasonable exposure times are about 1–100 ms for a single spot or the scanning speeds are about 1–50 μm/s for patterns.

First of all, the optically induced thermal effect is demonstrated by the creation of Au NIs as a function of the scanning speed and of the laser power. In order to obtain a well-defined area of Au NPs, the raster scan is used by the DLW technique. **Figure 8(a)** shows the optical microscope image of the fabricated samples. As the laser exposure dose changes, the color of Au NIs samples changes, suggesting a variation of the NIs sizes. **Figure 8(b)** shows the SEM image confirming the creation of Au NPs, whose size was estimated by a histogram to be about 60 nm. **Figure 8(c)** shows the measured absorption spectra of the corresponding samples, obtained before and after light exposure. The plasmonic resonance peak is clearly observed at a wavelength of about 550 nm.

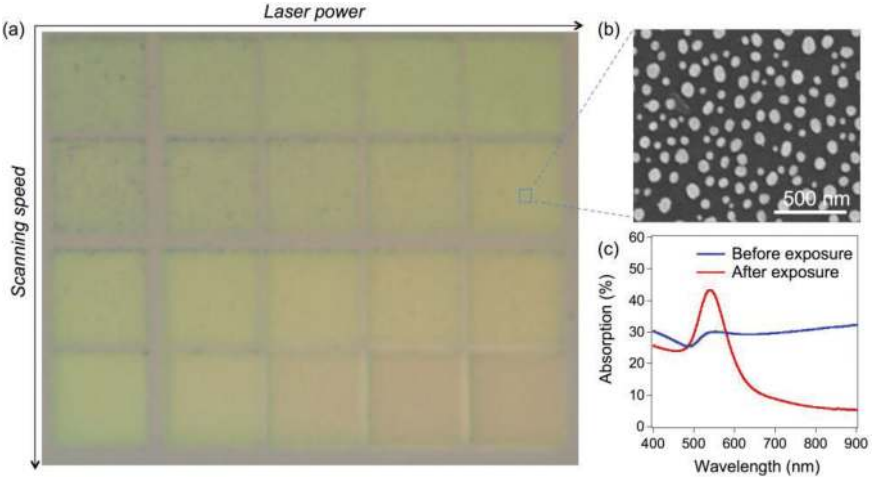

Figure 8. (a) Optical microscope image of Au NPs samples realized by using different exposure doses (laser powers and scanning speeds) of the DLW. (b) SEM image of Au NPs sample. (c) Experimental measurement of the plasmon resonance spectrum of the Au NSs obtained before and after laser exposure.

http://dx.doi.org/10.5772/intechopen.79236

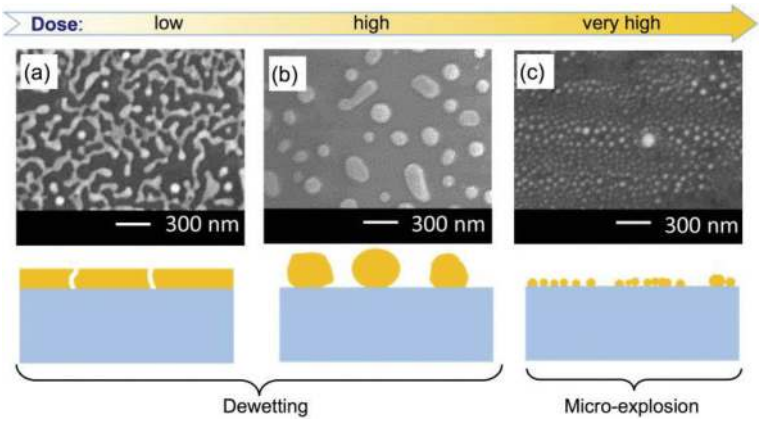

Figure 9. Dependence of the exposure dose on the formation of Au NPs. (a) SEM image of an Au discontinuous film, sputtered on a glass substrate. (b), (c) SEM images of Au NPs obtained by scanning a focused laser beam with a power of 40 mW and with scanning velocities of 20 μm/s (b) and 0.5 μm/s (c), respectively. Bottom line: Illustrations of Au film morphological transformation and mechanism as a function of the exposure dose.

It is worth to mention that there is some limit for the laser intensities, otherwise the induced temperature becomes too high, in particular after the formation of NPs, resulting in an explosion effect. **Figure 9** shows the effect of exposure dose, that is, laser intensity, on the formation of Au NPs. First, when the exposure dose is increased, the induced temperature increased resulting in the formation of well-separated Au NPs (**Figure 9(b)**). However, if the exposure dose increased strongly, the Au NPs exploded resulting in very small Au NPs (**Figure 9(c)**). When the laser intensity became too high, the Au material totally evaporated. Thus, by controlling the fabrication parameters, the morphology of Au NIs could be varied, which is quite important for further development of this method in various applications such as data storage, plasmonic band-pass filter, and color printing.

Indeed, thanks to the flexibility and versatility of the laser induced local thermal dewetting method, it is possible to write PNSs at high levels of complexities. **Figure 10** shows two

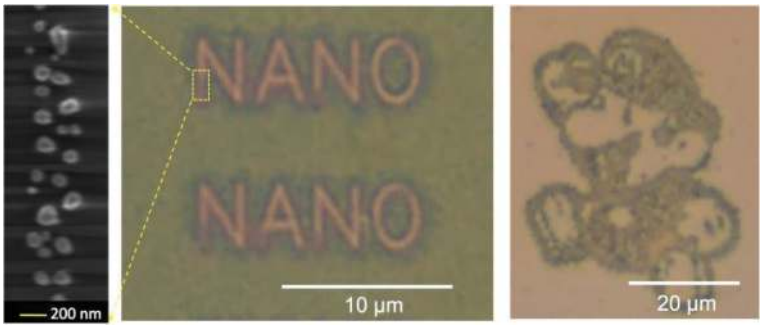

Figure 10. Optical microscope images of plasmonic patterns consist of Au NPs, realized by the optically induced thermal effect via DLW technique: "NANO" letter and "Mario" image. In the left: a SEM image of the Au NPs.

examples of the PNSs consisting of Au NIs: a "NANO" letter consisted of Au NPs as demonstrated by the SEM image and a "Mario" image consisted of Au NPs having different sizes, as seen by different colors.

4. Potential applications of fabricated plasmonic nanostructures

Nowadays, plasmonics appear in many different domains with numerous interesting applications and continue to attract more and more attention. Of course, these applications depend strongly on the fabrication technologies that may or may not allow to produce PNSs as desired. In this section, a few interesting applications related to PNSs fabricated by the DLW method will be presented, particularly for plasmonics-based sensor, optical filter, data storage, and color nanoprinter.

4.1. Applications of plasmonic nano-hole arrays

Figure 11(a) shows an experimental setup used to measure the transmission of NHAs fabricated previously by the indirect method. A supercontinuum laser (λ = 1200–1700 nm) is used as the illumination source. The beam was expanded and focused through NHA structure by an OL (NA = 0.4). The surrounding media of NHA can be easily changed from air to water

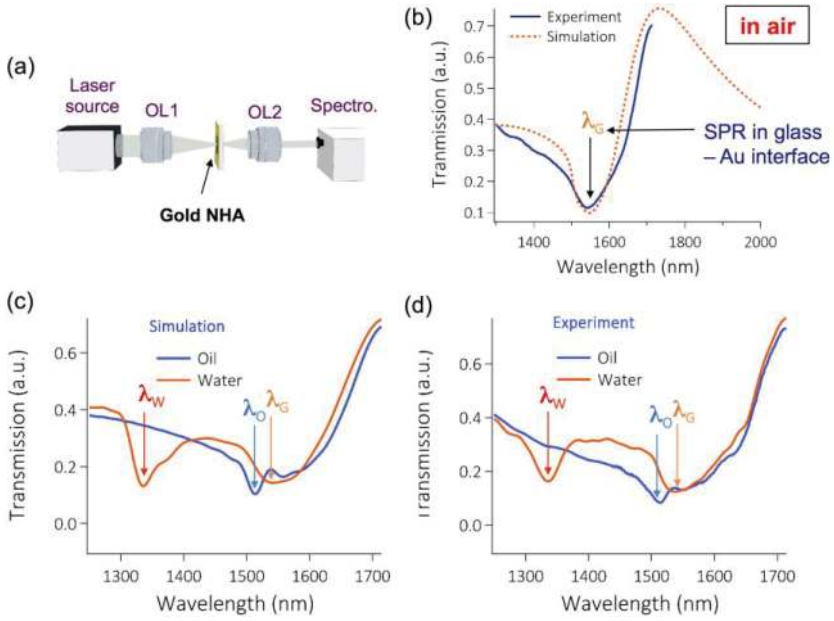

Figure 11. (a) Experimental setup of Au NHA transmission measurement. (b) Experimental and theoretical results of transmission spectra in air of fabricated Au NHA structures. (c) Experimental and (d) calculating transmission spectra of Au NHA structures in different media. For all simulations: Λ = 1000 nm, d_{hole} = 400 nm, t_{Au} = 50 nm, and t_{Cr} = 15 nm.

http://dx.doi.org/10.5772/intechopen.79236

and to oil by simply casting a drop of desired medium. The transmission spectra was collected by another OL and transmitted to a spectrometer. The experimental results were summarized and compared to predicted simulation results.

A remarkable similarity between experimental results and theoretical calculations is emphasized in **Figure 11(b)** for a sample immersed in air. We can observe a transmission dip around 1535 nm and a transmission peak located at about 1750 nm. The experimental transmission spectrum follows the evolution trend of calculation. However, due to the limitation of the detection range of the spectrometer, it is not possible to fully characterize this transmission band of the fabricated NHA, in particular, for the transmission peak. Therefore, the transmission dip corresponding to SPR band on the interface of gold-glass substrate is exploited further. From simulation (**Figure 11(c)**), a transmission dip is predicted approximately close to the wavelength of $\Lambda \times n$ with n as the refractive index of surrounding media, that is, transmission dips around 1330 and 1500 nm for water and oil, respectively. Those dips are effectively observed experimentally and shown in **Figure 11(d)**. The transmission dip at $\lambda_G \approx 1535$ nm (corresponding to SPR at glass-Au interface, called glass-mode) was unchanged in all three cases of water, oil, and air. Another dip appears at $\lambda_W \approx 1335$ nm when the NHA was embedded in water, called water-mode. This dip red-shifted to $\lambda_O \approx 1510$ nm when the NHA was immersed in oil, called oil-mode. This suggests a great application as plasmonics-based sensor if the surrounding medium of the NHA changes.

4.2. Plamonic-based data storage and color nanoprinters

The newly developed optically induced thermal effect by DLW technique allows imaging many applications at nanoscale. For a demonstration, different PNS were realized and several examples are shown in **Figure 12**. By this way, stereoscopic images can be encoded in the NSs and can be potentially used as elements for data storage and color nanoprinter applications. The stored data can be coded (binary code, alphabet letter, etc.) and programmed into the trajectory of laser scanning to directly write data on metallic materials.

Figure 12(a) shows an example of the "NANO LETTERS" words made by Au NIs. The height of the word can be as small as 1 μm. Generally, any nano text can be written by this DLW

Figure 12. (a) Optical microscope image of the plasmonic text ("NANO LETTERS" with different sizes) realized by the DLW technique. (b) Optical image of a quick response (QR) code, which links to the website of the author's laboratory (LPQM).

method and read by plasmonic effect. **Figure 12(b)** illustrates a quick response (QR) code, which links to the website of the author's laboratory (LPQM). Bar code (1D) or QR code (2D) is a fast, easy, and accurate data storage method enabling products to be tracked efficiently and accurately. In particular, QR code attracts more attention in e-commerce because it also improves mobile user experience by convenient and easy operation.

Furthermore, as mentioned previously, the DLW technique allows production of any structures at nanoscale. **Figure 13** shows the result of a real image: a real "experiment book" of French laboratories. The real photo was imported to a MATLAB image, and each pixel was transferred to an exact dose of the light exposure, resulting in a plasmonic image of this "experiment book" at microscale. The image color is quite faithful to the original one, but theoretically and experimentally limited in the green and yellow color domain. That could be explained by the result shown in the simulation section, which predicted that the plasmonic resonance shifts only about 48 nm when the particles size changes from 20 to 100 nm. It is theoretically expected that a variety of colors could be obtained by organizing these Au NIs in order, like 1D and 2D PNSs [10, 11]. The combination of LSPR and PNS will offer a large possibility to tune the color.

4.3. About resonantly enhanced plasmonic magneto-optics

The magneto-optical (MO) sensors are a powerful sensing platform based on the Faraday or Kerr effects, that is, the rotation of linearly polarized light when it passes through or reflects from a magnetic thin film under influence of an external magnetic field [40]. However, conventional MO sensor cannot be used as a refractometer since it is not sensitive to minute

Figure 13. The color printed image fabricated by the DLW method on Au film. Left: a real "experiment book". Right: a plasmonic image of corresponding book at microscale.

http://dx.doi.org/10.5772/intechopen.79236

changes of refractive index; therefore, such a sensor is not suitable for gas, chemical, and biological sensing applications. Recently, it has been discovered that when the MO active media is coupled with PNSs, the strong local EM fields produced through LSPR or SPP interact strongly with ambient magnetic materials. Consequently, the MO property of the magnetic media could be significantly enhanced at these LSPR/SPP resonance wavelengths [41, 42]. Since magnetic materials possess weak plasmonic property, most current PMO materials for sensors are layered films made by noble metal (Au, Al, and Ag) films and magnetic (Ni, Co, Fe, or magnetic insulators) films [43]. The DLW method is an excellent tool for fabrication on demand of arbitrary NHAs, whose plasmonic property and hence PMO performance may be significantly enhanced. It is expected that the PMO sensors have advantages over the corresponding plasmonic sensors and will be fully explored.

5. Conclusion

In summary, this chapter reports systematically most aspects related to arbitrary plasmonic nanostructures, in particular those realized by the direct laser writing technique. In the first section, the optical properties of very basic nanostructures are completely investigated by using a well-known FDTD simulation method. Real fabricated metallic structures are also imported to a simulation model and calculated accurately. These investigations offer a short but understandable image of plasmonic properties of various nanostructures and guide for applications of plasmonic nanostructures in different domains. In the second section, the direct laser writing technique is demonstrated as an excellent method for realization of desired plasmonic nanostructures on demand. The fabrication of plasmonic nanostructures is demonstrated in two ways: indirectly via the use a polymeric template and directly by exploiting the optically induced local thermal effect. Any plasmonic microstructures with desired size, shape, and color were obtained by controlling the writing pattern and the exposure doses (laser power and writing speed). Finally, several important applications of plasmonic nanostructures, in particular those realized by direct laser writing method, have been demonstrated. Namely, the nano-holes arrays are demonstrated as excellent optical bandpass filters and also sensitive plasmonics-based sensor. The plasmonic nano-islands realized by optically induced thermal effect offered an excellent way for data storage and color nanoprinter. It is clear that those fabricated structures could be useful for a wide range of applications in numerous fields (physics, chemistry, biology, etc.).

Acknowledgements

This work is supported by a public grant overseen by the French National Research Agency (ANR) (project: GRATEOM) and by a public grant of Ministry of Science and Technology of Vietnam (project: DTDLCN.01/2017).

Author details

Quang Cong Tong[1,2], Fei Mao[1], Mai Hoang Luong[1,3], Minh Thanh Do[1,4], Rasta Ghasemi[5], Tran Quoc Tien[2], Tho Duc Nguyen[3] and Ngoc Diep Lai[1]*

*Address all correspondence to: ngoc-diep.lai@ens-paris-saclay.fr

1 Laboratoire de Photonique et Moléculaire, UMR 8537, Ecole Normale Supérieure de Cachan, CentraleSupélec, CNRS, Université Paris-Saclay, Cachan, France

2 Institute of Materials Sciences, Vietnam Academy of Science and Technology, Hanoi, Vietnam

3 Department of Physics and Astronomy, University of Georgia, Athens, Georgia, USA

4 Hanoi National University of Education, Hanoi, Vietnam

5 Institute D'Alembert, Ecole Normale Supérieure Paris-Saclay, Cachan, France

References

[1] Wood RW. On a remarkable case of uneven distribution of light in a diffraction grating spectrum. The London, Edinburgh, and Dublin philosophical magazine and. Journal of Science. 1902;**4**:396-402. DOI: 10.1080/14786440209462857

[2] Maier SA. Plasmonics: Fundamentals and Applications. New York Inc.: Springer Science & Business Media; 2007. DOI: 10.1007/0-387-37825-1

[3] Stewart ME, Anderton CR, Thompson LB, Maria J, Gray SK, Rogers JA, Nuzzo RG. Nanostructured plasmonic sensors. Chemical Reviews. 2008;**108**:494-521. DOI: 10.1021/cr068126n

[4] Halas NJ, Lal S, Chang WS, Link S, Nordlander P. Plasmons in strongly coupled metallic nanostructure. Chemical Reviews. 2011;**111**:3913-3961. DOI: 10.1021/cr200061k

[5] Hutter E, Fendler JH. Exploitation of localized surface plasmon resonance. Advanced Materials. 2004;**16**:1685-1706. DOI: 10.1002/adma.200400271

[6] Homola J, Yee SS, Gauglitz G. Surface plasmon resonance sensors: review. Sensors and Actuators B: Chemical. 1999;**54**:3-15. DOI: 10.1016/S0925-4005(98)00321-9

[7] Jimenez de Aberasturi D, Serrano-Montes AB, Liz-Marzán LM. Modern applications of plasmonic nanoparticles: From energy to health. Advanced Optical Materials. 2015;**3**:602-617. DOI: 10.1002/adom.201500053

[8] Barnes WL, Dereux A, Ebbesen TW. Surface plasmon subwavelength optics. Nature. 2003;**424**:824-830. DOI: 10.1038/nature01937

[9] Ringler M, Schwemer A, Wunderlich M, Nichtl A, Kurzinger K, Klar TA, Feldmann J. Shaping emission spectra of fluorescent molecules with single plasmonic nanoresonators. Physical Review Letters. 2008;**100**:203002. DOI: 10.1103/PhysRevLett.100.203002

[10] Wang X, Gogol P, Cambril E, Palpant B. Near- and far-field effects on the plasmon coupling in gold nanoparticle arrays. Journal of Physical Chemistry C. 2012;**116**:24741-24747. DOI: 10.1021/jp306292r

[11] Chanda D, Shigeta K, Truong T, Lui E, Mihi A, Schulmerich M, Braun PV, Bhargava R, Rogers JA. Coupling of plasmonic and optical cavity modes in quasi-three-dimensional plasmonic crystals. Nature Communications. 2011;**2**:479. DOI: 10.1038/ncomms1487

[12] Zijlstra P, Chon JWM, Gu M. Five-dimensional optical recording mediated by surface plasmons in gold nanorods. Nature. 2009;**459**:410-413. DOI: 10.1038/nature08053

[13] Brongersma ML, Kik PG, editors. Surface Plasmon Nanophotonics. Vol. 131. Springer Series in Optical Sciences. Netherlands: Springer; 2007. 268 p. DOI: 10.1007/978-1-4020-4333-8

[14] Enoch S, Nicolas B, editors. Plasmonics: From Basics To Advanced Topics. Springer Series in Optical Sciences. Vol. 167. Berlin Heidelberg: Springer-Verlag; 2012. 321 p. DOI 10.1007/978-3-642-28079-5

[15] Bozhevolnyi SI, Martin-Moreno L, Garcia-Vidal F, editors. Quantum Plasmonics. Vol. 185. Springer Series in Solid-State Sciences. Switzerland: Springer International Publishing; 2017. 327 p. DOI 10.1007/978-3-319-45820-5

[16] Shahbazyan TV, Stockman MI, editors. Plasmonics: Theory and Applications. Springer Series in Challenges and Advances in Computational Chemistry and Physics. Vol. 15. Netherlands: Springer; 2013. 577 p. DOI 10.1007/978-94-007-7805-4

[17] Courant R, Friedrichs K, Lewy H. Über die partiellen Differenzengleichungen der mathematischen Physik. Mathematische Annalen. 1928;**100**:32-74. DOI: 10.1007/BF01448839

[18] Taflove A, Hagness SC, editors. Computational Electrodynamics: The Finite-Difference Time-Domain Method. 2nd ed. Norwood MA: Artech House; 1995. 1006 p

[19] Do MT, Tong QC, Luong MH, Lidiak A, Ledoux- Rak I, Lai ND. Fabrication and characterization of large-area unpatterned and patterned plasmonic gold nanostructures. Journal of Electronic Materials. 2016;**45**:2347-2353. DOI: 10.1007/s11664-015-4291-6

[20] Palik ED editor. Handbook of Optical Constants of Solids. USA: Academic Press; 1985. 804 p

[21] Johnson PB, Christy RW. Optical constants of the noble metals. Physical Review B. 1972; **6**:4370. DOI: 10.1103/PhysRevB.6.4370

[22] Turkevich J, Stevenson PC, Hillier J. A study of the nucleation and growth process in the synthesis of colloidal gold. Discussions of the Faraday Society. 1951;**11**:55-75. DOI: 10.1039/DF9511100055

[23] Brust M, Walker M, Bethell W, Schriffin DJ, Whyman R. Synthesis of thiol-derivatised gold nanoparticles in a two phase liquid system. Journal of the Chemical Society, Chemical Communications. 1994;**0**:801-802. DOI: 10.1039/C39940000801

[24] Xu ZC, Shen CM, Xiao CW, Yang TZ, Zhang HR, Li JQ, Li HL, Gao HJ. Wet chemical synthesis of gold nanoparticles using silver seeds: A shape control from nanorods to hollow spherical nanoparticles. Nanotechnology. 2007;**18**:115608. DOI: 10.1088/0957-4484/18/11/115608

[25] Karakouz T, Tesler AB, Bendikov TA, Vaskevich A, Rubinstein I. Highly stable localized plasmon transducers obtained by thermal embedding of gold island films on glass. Advanced Materials. 2008;**20**:3893-3899. DOI: 10.1002/adma.200703092

[26] Gupta G, Tanaka D, Ito Y, Shibata D, Shimojo M, Furuya K, Mitsui K, Kajikawa K. Absorption spectroscopy of gold nanoisland films: Optical and structural characterization. Nanotechnology. 2009;**20**:025703. DOI: 10.1088/0957-4484/20/2/025703

[27] Kang M, Park S, Jeong K. Repeated solid-state dewetting of thin gold films for nanogap-rich plasmonic nanoislands. Scientific Reports. 2015;**5**:14790. DOI: 10.1038/srep14790

[28] Axelevitch A, Apter B, Golan G. Simulation and experimental investigation of optical transparency in gold island films. Optics Express. 2013;**21**:4126-4138. DOI: 10.1364/OE.21.004126

[29] Ozhikandathil J, Packirisamy M. Simulation and implementation of a morphology-tuned gold nano-islands integrated plasmonic sensor. Sensors. 2014;**14**:10497-10513. DOI: 10.3390/s140610497

[30] Xu T, Wu YK, Luo X, Guo LJ. Plasmonic nanoresonators for high-resolution colour filtering and spectral imaging. Nature Communications. 2010;**1**:59. DOI: 10.1038/ncomms1058

[31] Cheng F, Gao J, Luk TS, Yang X. Structural color printing based on plasmonic metasurfaces of perfect light absorption. Scientific Reports. 2015;**5**:11045. DOI: 10.1038/srep11045

[32] Wang X, Palpant B. Large and ultrafast optical response of a one-dimensional plasmonic-photonic cavity. Plasmonics. 2013;**8**:164-1653. DOI: 10.1007/s11468-013-9583-1

[33] Daghestani HN, Day BW. Theory and applications of surface plasmon resonance, resonant mirror, resonant waveguide grating, and dual polarization interferometry biosensors. Sensors. 2010;**10**:9630-9646. DOI: 10.3390/s101109630

[34] Ebbesen TW, Lezec HJ, Ghaemi H, Thio T, Wolff R. Extraordinary optical transmission through sub-wavelength hole arrays. Nature. 1998;**391**:667-669. DOI: 10.1038/35570

[35] Grigorenko AN, Geim AK, Gleeson HF, Zhang Y, Firsov AA, Khrushchev IY, Petrovic J. Nanofabricated media with negative permeability at visible frequencies. Nature. 2005;**438**:355-338. DOI: 10.1038/nature04242

[36] Steinbruck A, Choi JW, Fasold S, Menzel C, Sergeyev A, Pertsch T, Grange R. Plasmonic heating with near infrared resonance nanodot arrays for multiplexing optofluidic applications. RSC Advances 2014;**4**:898. DOI: 10.1039/C4RA13312A

[37] Tong QC, Luong MH, Tran TM, Remmel J, Do MT, Kieu DM, Ghasemi R, Nguyen DT, Lai ND. Realization of desired plasmonic structures via a direct laser writing technique. Journal of Electronic Materials. 2017;**46**:3695-3701. DOI: 10.1007/s11664-016-5131-z

[38] Tong QC, Luong MH, Remmel J, Do MT, Nguyen DTT, Lai ND. Rapid direct laser writing of desired plasmonic nanostructures. Optics Letters. 2017;**42**:2382. DOI: 10.1364/OL.42.002382

[39] Li Q, Do MT, Ledoux-Rak I, Lai ND. Concept for three-dimensional optical addressing by ultralow one-photon absorption method. Optics Letters. 2013;**38**:4640-4643. DOI: 10.1364/OL.38.004640

[40] Scott G, Lacklison D. Magnetooptic properties and applications of bismuth substituted iron garnets. IEEE Transactions on Magnetics. 1976;**12**:292-311. DOI: 10.1109/TMAG.1976.1059031

[41] Armelles G, Cebollada A, García-Martín A, González MU. Magnetoplasmonics: Combining magnetic and plasmonic functionalities. Advanced Optical Materials. 2013;**1**:10-35. DOI: 10.1002/adom.201200011

[42] Clavero C, Yang K, Skuza JR, Lukaszew RA. Magnetic field modulation of intense surface plasmon polaritons. Optics Express. 2010;**18**:7743-7752. DOI: 10.1364/OE.18.007743

[43] Escobedo C. On-chip nanohole array based sensing: A review. Lab on a Chip. 2013;**13**:2445-2463. DOI: 10.1039/C3LC50107H